Progress in DMAPS developments and first tests of the Monopix2 chips in 150 nm LFoundry and 180 nm TowerJazz technology

J. Dingfelder, M. Barbero, P. Barrillon, I. Berdalovic, C. Bespin, P. Breugnon, I. Caicedo, R. Cardella, Y. Degerli, L. Flores Sanz de Acedo, et al.

Progress in DMAPS developments and first tests of the Monopix2 chips in 150 nm LFoundry and 180 nm TowerJazz technology

J. Dingfelder[a], M. Barbero[b], P. Barrillon[b], I. Berdalovic[d], I. Bespin[a], P. Breugnon[b], I. Caicedo[a], R. Cardella[d], Y. Degerli[c], L. Flores Sanz de Acedo[d], F. Guilloux[c], A. Habib[b], T. Hirono[a], T. Hemperek[a], F. Hügging[a], H. Krüger[a], T. Kugathasan[d], K. Moustakas[a], P. Pangaud[b], H. Pernegger[d], F. Piro[d], D.-L. Pohl[a], P. Riedler[d], A. Rozanov[b], P. Rymaszewski[a], P. Schwemling[c], W. Snoeys[d], T. Wang[a], N. Wermes[a], S. Zhang[a]

[a] *Universität Bonn, Physikalisches Institut, Nußallee 12, 53115 Bonn, Germany*
[b] *Aix Marseille University CNRS/IN2P3, CPPM, 163 Avenue de Luminy, 13009 Marseille, France*
[c] *IRFU, CEA-Saclay, 91191 Gif-sur-Yvette, France*
[d] *CERN, Espl. des Particules 1, 1211 Meyrin, Switzerland*

Abstract

Depleted Monolithic Active Pixel Sensors (DMAPS) are monolithic pixel detectors with high-resistivity substrates designed for use in high-rate and high-radiation environments. They are produced in commercial CMOS processes, resulting in relatively low production costs and short turnaround times, and offer a low material budget. LF-Monopix1 and TJ-Monopix1 are large DMAPS prototypes produced in 150 nm LFoundry and 180 nm TowerJazz technology, respectively, that follow two different design concepts regarding the charge collection electrode. Prototypes of both development lines have been extensively tested and characterized over the last years. The second-generation Monopix prototypes, Monopix2, were recently produced. They were designed to address the shortcomings of their predecessors, in particular related to radiation hardness and cross talk, and further improve upon their performance. The latest measurements with LF-Monopix1 and TJ-Monopix1 concerning hit efficiency, depletion, and radiation hardness as well as the initial test results of the new Monopix2 prototypes are presented.

Keywords: Pixel detector, monolithic pixel, DMAPS, CMOS sensor, radiation

hardness

1. Introduction

In monolithic pixel detectors, the sensor and the readout electronics form an entity that is fabricated in the same silicon substrate using a commercial CMOS process. As compared to the hybrid pixel detector technology, which is still the standard in current particle physics experiments and provides excellent rate capabilities and radiation tolerance, monolithic pixel detectors offer a low material budget and make the labor- and cost-intensive bump bonding process to connect sensor and readout chip unnecessary [1]. A challenge for the design of monolithic detectors is to decouple the charge collection from the high-frequency switching processes of the electronics and to reach sufficiently large charge collection efficiencies in high-radiation environments, as expected for instance at the HL-LHC.

Improved radiation tolerance can be achieved with Depleted Monolithic Active Pixel Sensors (DMAPS) that use high-ohmic substrates ($\rho > 1\ \mathrm{k\Omega\,cm}$) and large enough bias voltages to facilitate full depletion of the substrate (depletion depth $d \propto \sqrt{\rho V_{\mathrm{bias}}}$) and fast charge collection by drift. Large-scale DMAPS prototype chips have been designed in various CMOS technologies with integrated fast readout electronics [2–4]. The two DMAPS development lines LF-Monopix and TJ-Monopix, fabricated in 150 nm LFoundry and 180 nm TowerJazz technology, respectively, feature different pixel layouts (in particular concerning the size of the collection electrode), front-end implementations and biasing schemes while using the same readout architecture. They were initially developed to comply with the requirements of the outer layer of the ATLAS Inner Tracker upgrade [5], but have a broad range of potential applications in particle physics, for instance for an upgrade of the Belle II experiment in Japan, and as imaging sensors.

During the last few years, the first-generation prototypes LF-Monopix1 and TJ-Monopix1 have been extensively tested and characterized. Improved second-

generation prototypes, Monopix2, were submitted for both DMAPS lines in 2020 and became available for testing in spring 2021. In this contribution, recent updates on the Monopix1 characterizations and the first test results of the new Monopix2 prototypes are presented.

2. The Monopix chips

LF-Monopix and TJ-Monopix are both fully monolithic pixel designs with the readout electronics completely integrated in the pixel cell, but follow different concepts for the charge collection electrode. LF-Monopix features a large electrode that surrounds the electronics, while TJ-Monopix has a small collection electrode with the electronics placed outside of the electrode. Both chips use a fully synchronous column-drain readout architecture [6] that is similar to the one used in the FE-I3 readout chip of the ATLAS pixel detector [7]. Charges that are created in the sensitive volume by a traversing ionizing particle are collected in the collection electrode, amplified and converted into a voltage pulse that is compared to an adjustable threshold. The leading and trailing edges of the discriminator output determine the time of arrival and the total length (time over threshold) of the pulse using a 40 MHz clock.

2.1. LF-Monopix design (LFoundry 150 nm)

LF-Monopix1 is the first large-scale DMAPS prototype with a large collection electrode and fully integrated electronics for fast standalone readout [8]. The pixel matrix has a size of 1×1 cm^2 and a pitch of 50×250 μm^2. A cross section of the pixel layout is shown in Fig. 1. The collection electrode is formed by a large deep n-implant that contains the in-pixel electronics, while being isolated from it through a p-type implant. A p-type substrate with a high resistivity (> 2 $k\Omega\,$cm) constitutes the sensitive volume, which can be fully depleted if a large enough bias voltage is applied. After wafer thinning and back-side processing, substrate thicknesses ranging from 750 μm down to 100 μm are available. The large electrode and strong electric field lead to short drift times

that result in a high charge collection efficiency and a good radiation tolerance. On the other hand, the large sensor capacitance ($\sim$ 400 fF) related to the size of the electrode compromises the noise and rise time of the signal (more power for the analog front-end is needed to maintain a good timing performance) and requires special design efforts to reduce cross talk from digital activity into the sensing node. Detailed results of the characterization of LF-Monopix1 can be found in Refs. [2, 9–12].

The successor chip LF-Monopix2 has a size of 1×2 cm^2, i.e. full column length, and a smaller pixel pitch of 50×150 μm^2. The pixel matrix takes up 82% of the chip area, the rest is occupied by guard rings, decoupling capacitors and peripheral circuitry at the top and bottom of the chip. Due to the smaller pixel size and hence reduced capacitance ($\sim 250 - 300$ fF) an improved signal-to-noise ratio and a better timing performance are expected. A problem with spurious signals caused by cross talk related to switching of the digital read signal that was observed with LF-Monopix1 was addressed by improving the substrate potential connection inside the pixel and the shielding of the sensing node from transients in V_{DD} lines caused by fast switching signals. A fast and radiation-hard combination of preamplifier and discriminator was chosen as main front-end implementation, based on performance measurements of the first prototype. In addition, variations of such front-end and the chip's tuning circuitry were designed to further improve the timing and threshold dispersion. The matrix is divided into three main submatrices that include different charge sensitive amplifier (CSA) designs. One of the submatrices is further subdivided into four regions with different CSA feedback capacitances (1.5 fF or 5.0 fF), local threshold tuning schemes (unidirectional or bidirectional) and pixel-level logic. The pixel design of LF-Monopix2 features rounded corners for reduction of the electric field on the edges, which together with an optimized guard-ring design improve the breakdown behavior of the sensor.

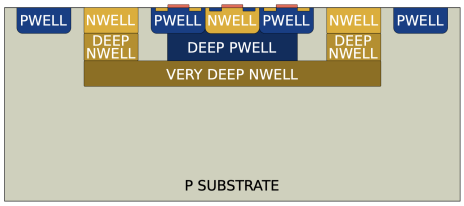

Figure 1: Schematic pixel cross section of LF-Monopix. The deep n-implant forms the charge collection electrode.

2.2. TJ-Monopix design (TowerJazz 180 nm)

The TJ-Monopix series is based on a small collection electrode design [12–14]. The TJ-Monopix1 chip has an area of 1×2 cm^2 and a pixel pitch of 36×40 μm^2. A small n-well is used as collection electrode and separated from the area where the in-pixel electronics is implemented (Fig. 2). A 25 μm thick p-type epitaxial layer with a resistivity of more than 1 kΩ cm grown on a low-resistivity substrate serves as sensitive volume. A deep p-well shields the n-wells of the PMOS transistors and isolates them from the charge collection node, thus facilitating full CMOS logic. One of the main advantages of this pixel geometry is the small sensor capacitance ($\sim 3-4$ fF), which facilitates low noise levels and fast timing while keeping the power consumption minimal. In addition, cross talk is substantially reduced. However, the small-electrode design is generally less radiation-hard due to longer drift times and regions with low electric field. A modified CMOS process [15] with a low-dose n-type layer added over the full pixel area improves the charge collection and is used to achieve full depletion of the epitaxial layer with small reverse bias voltages, thus enhancing radiation hardness [16]. Since the hit efficiency after radiation damage turned out to be still too low, additional implant modifications (n-gap or extra deep p-well) for lateral field enhancement [17] or the use of a thick Czochralski substrate to obtain a larger charge signal [18] were implemented and tested. Their effect is discussed in Section 3.2.1. The TJ-Monopix1 chip has been characterized in a series of measurements and the results can be found in Refs. [9, 10, 12].

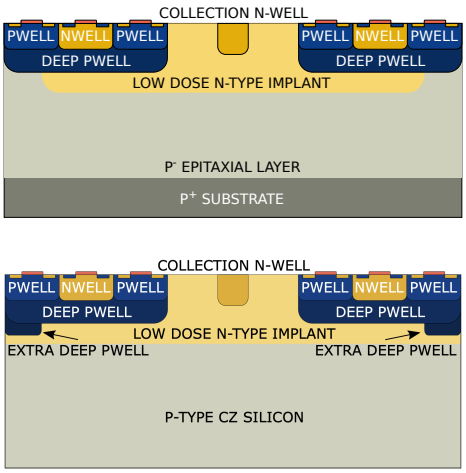

Figure 2: Schematic pixel cross section of TJ-Monopix. The small n-well separated from the readout electronics forms the charge collection electrode. Two process modifications are shown with p-epitaxial layer and n-gap on the pixel edges (top) and with p-type Czochralski substrate and extra deep p-well (bottom).

TJ-Monopix2 is a full-size (2×2 cm^2) chip designed to address the shortcomings of TJ-Monopix1 and provide more sophisticated periphery and LVDS communication. The active area of TJ-Monopix2, which corresponds to about 70% of the chip area, contains 512×512 pixels with a size of 33.04×33.04 μm^2. In addition to the ca. 25% smaller pixel size, which results in faster charge collection, improvements in the analog front end make a reduction of the operating threshold by about a factor of 3 (below 200 e^-) possible. An increased coupling capacitor as well as larger transistors are expected to yield higher gain, lower noise and improved TID tolerance. The significantly lower threshold enables the detection of small charge depositions (e.g. because of charge sharing or trapping) in the thin epitaxial layer. The Monopix2 chip contains four different front-end flavors: DC-coupled pixels with diode input reset and AC-coupled pixels with front-side HV biasing, both with or without an extra cascode transistor to increase the preamplifier gain. The new front-end circuit design reduces the noise by approx. 40% and the threshold dispersion by $80 - 90$%, depending

on the flavor [14]. Additional new functionalities were introduced such as improved pixel masking by using individual in-pixel configuration memory and a (3-bit) threshold tuning on pixel level to allow for a more uniform threshold distribution over the matrix.

3. Measurements

3.1. Results for LF-Monopix

3.1.1. Measurements with irradiated LF-Monopix1 chips

In a previous measurement with unthinned (750 μm) LF-Monopix1 chips, the hit efficiency after irradiation with neutrons up to a fluence of $10^{15} n_{eq}\mathrm{cm}^{-2}$ was determined to be 98.9% [2] for a threshold of 1600 e^- and a bias voltage of 130 V. The efficiency has now also been measured for a backside-processed chip thinned down to 100 μm (of which 85 μm correspond to depletable silicon substrate). The measurement was performed with a bias voltage of 60 V (160 V) for the unirradiated (irradiated) case. The hit efficiency maps are shown in Fig. 3. Efficiencies of 99.6% (99.4%) before (after) neutron irradiation were obtained for the 100 μm thick sensor. Since this measurement was performed with the same front-end flavor that serves as default for LF-Monopix2, a similar efficiency may also be expected for the new chip.

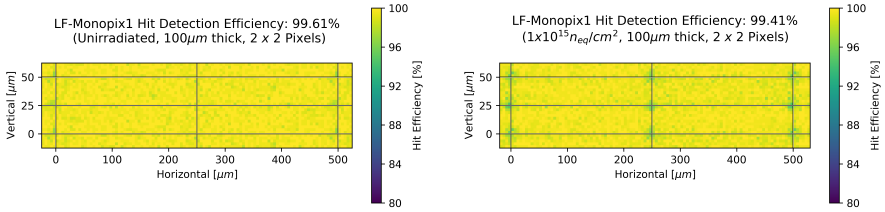

Figure 3: Hit efficiency, mapped onto a 2×2 pixel area, for LF-Monopix1 thinned down to 100 μm, measured for an unirradiated chip (left) and after neutron irradiation up to a fluence of $10^{15} n_{eq}\mathrm{cm}^{-2}$ (right).

The full depletion voltage for the 100 μm thick silicon substrate used in both LF-Monopix chips has been determined from a measurement of the most probable value of the deposited charge distribution for minimum ionizing particles (MIPs) in dependence of the applied bias voltage. As can be seen in Fig. 4, full depletion is reached for bias voltages of $\sim$ 15 V before and $\sim$ 150 V after irradiation. The maximum achievable charge for the neutron-irradiated sample was found to be somewhat higher than for the unirradiated sample. This could be due to chip-to-chip variations in thickness after wafer thinning or charge multiplication occurring in a fully depleted thin sensor after exposure to severe hadron fluences, but these hypotheses still require further investigation.

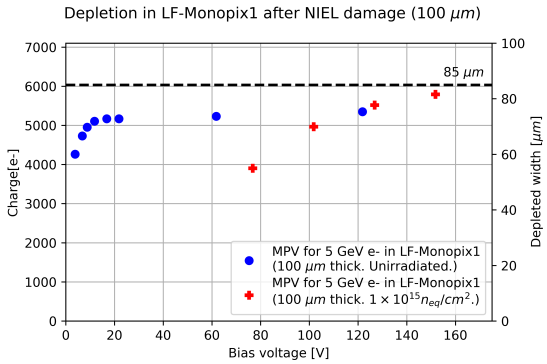

Figure 4: Depletion of LF-Monopix1 (100 μm, unirradiated and neutron-irradiated to $10^{15} n_{eq}\mathrm{cm}^{-2}$) determined from the most probable value (MPV) of the charge distribution of traversing MIPs in dependence of the applied bias voltage.

3.1.2. First measurements with LF-Monopix2: Readout, leakage current, noise and threshold

The new digital in-pixel injection circuitry implemented in LF-Monopix2 was used to validate the readout architecture and the response of the analog front end. A measurement of the CSA response as a function of injected charge is shown in Fig. 5. A linear response is observed and a gain of $\sim$ 20 $\mu\mathrm{V}/e^-$ is measured by looking directly at the analog output of the CSA. The correct

column-drain readout for the full-length column could successfully be demonstrated.

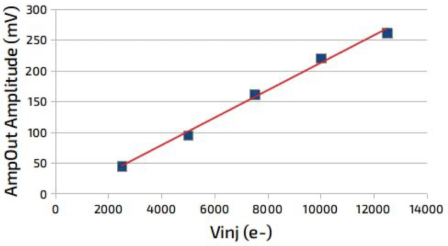

Figure 5: Measured CSA output as a function of injected charge for LF-Monopix2.

A measurement of the leakage current as a function of bias voltage was performed at room temperature for unthinned (750 μm thick) sensors. No breakdown was observed for LF-Monopix2 up to the maximum applied bias voltage of 320 V, as can be seen in Fig. 6. For comparison, the breakdown voltage measured for a LF-Monopix1 chip of the same thickness is about 280 V. This demonstrates the effectiveness of the optimized guard-ring structure, which includes an increased ring spacing and an addition of p-type material to the rings to reduce the voltage drop in each of them.

First noise and threshold measurements for LF-Monopix2 were carried out. Threshold scans were performed by repeatedly injecting varying amounts of charge and counting the number of registered pixel hits. Threshold and ENC are extracted from a fit to the measured S-curves. The threshold is defined as the charge, for which 50% of the injections are observed as hits. The ENC was determined to be $90 - 100\,e^-$ (Fig.7) with a dispersion of $15 - 20\,e^-$. The minimum threshold was found to be approximately $1000\,e^-$. The noise is about 30% lower than for LF-Monopix1, which meets the expectation. Since it was measured with the same front-end flavor for both chips, most of the improvement in ENC mean and dispersion should come from the reduced detector capacitance.

The results of the measurements that have been performed with LF-Monopix2 so far are summarized in Tab. 1 and compared to the expected values and the

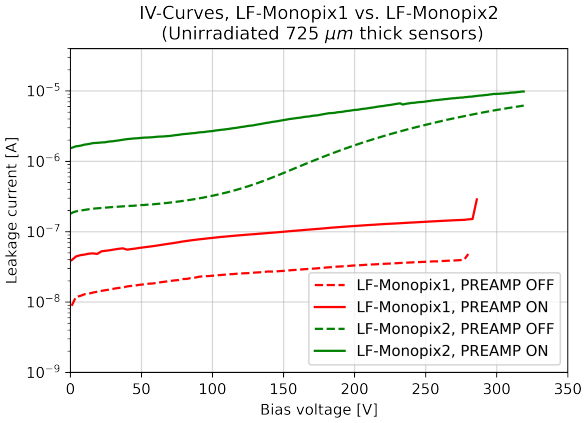

Figure 6: Comparison of I-V curves for LF-Monopix1 and LF-Monopix2 (backside-processed, 750 μm thick sensors). The higher level of leakage current for LF-Monopix2 in this plot is mainly due to the larger number of pixels.

ones measured for LF-Monopix1.

3.2. Results for TJ-Monopix

3.2.1. Hit efficiency of irradiated TJ-Monopix1

While the measurements performed with TJ-Monopix1 have generally shown promising results, radiation hardness is still an issue. It was seen that after neutron-irradiation up to $10^{15} n_{eq}\mathrm{cm}^{-2}$, the hit efficiency is only about 70% [9], which is partially due to charge losses in the weak lateral electrical field under the deep p-well. As mentioned in Sec. 2.2, this problem was addressed by introducing a gap in the n-implant used for full depletion or an additional p-implant in this region to enhance the charge collection [17]. Moreover, an increase of the charge signal would be beneficial and can be achieved through use of a thick Czochralski substrate instead of a thin epitaxial layer (cf. Fig. 2).

Two such sensor variants with (1) 30 μm epitaxial layer and n-gap and (2) 300 μm Czochralski substrate and extra deep p-well were studied. Since the modifications with n-gap and extra deep p-well serve the purpose of enhancing radiation tolerance similarly well, as was illustrated in Ref. [19], a comparison

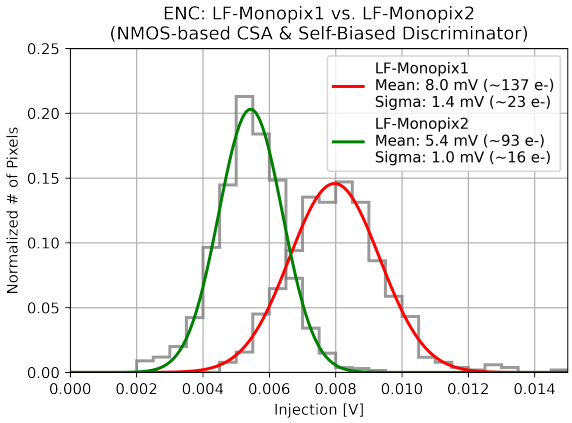

Figure 7: Normalized ENC distribution for LF-Monopix1 and LF-Monopix2.

of these two sensor variants mainly corresponds to a study of the effect of the thickness of the sensitive volume. The two sensor variants were irradiated with neutrons at the TRIGA reactor in Ljubljana and taken to a test-beam campaign with a 5 GeV electron beam at DESY. The hit efficiency maps, where the efficiencies obtained for all pixels have been projected onto a 2×2 pixel area, are shown in Fig. 8. As expected, the charge loss appears mostly in the pixel corners, where charge sharing is most prominent, while the efficiencies in the central pixel regions are only reduced by a few percent. The first variant with 30 μm epitaxial layer shows an increased efficiency of 87.1% after irradiation with neutrons up to $10^{15} n_{eq}\mathrm{cm}^{-2}$, illustrating the improvement due to the n-gap. The second variant with 300 μm Czochralski substrate yields an efficiency of 98.6%. The larger amount of charge deposited in the thicker sensitive volume thus leads to the expected significant improvement in hit efficiency. It can thus be concluded that the sensor can be made efficient after radiation damage by making the sensitive volume thicker or by lowering the minimum achievable threshold through front-end optimization.

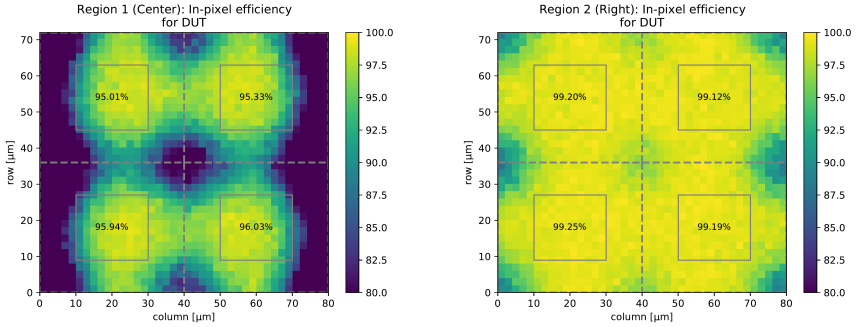

Figure 8: Hit efficiency for TJ-Monopix1 after neutron irradiation to $10^{15} n_{eq}\mathrm{cm}^{-2}$, mapped onto a 2×2 pixel area. Two different sensor variants are shown. Left: 30 μm epitaxial layer and n-gap (threshold: $450\,e^-$), right: 300 μm Czochralski substrate and extra deep p-well (threshold: $490\,e^-$).

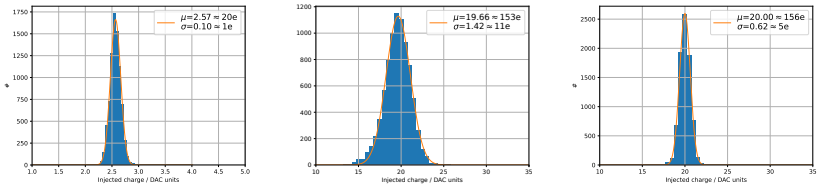

Figure 9: ENC distribution (left) and threshold distribution before (middle) and after local tuning (right) for TJ-Monopix2. The means (μ) and standard deviations (σ) obtained from Gaussian fits are given in the legends in units of electrons.

3.2.2. Noise and threshold for TJ-Monopix2

To achieve sufficient radiation hardness for a sensor with epitaxial layer, the threshold needs to be significantly reduced. The in-pixel threshold tuning, which was implemented as a new feature in TJ-Monopix2, helps to minimize the thresholds dispersion. Threshold scans were performed in the same way as explained in Sec. 3.1.2. A mean ENC of $20\,e^-$ with a dispersion of $1\,e^-$ and a threshold of $156\,e^-$ with a dispersion of $5\,e^-$ after threshold tuning are measured, which represent a significant improvement compared to TJ-Monopix1. Figure 9 compares the threshold distributions obtained before and after tuning. The in-

Table 1: Overview of measured performance parameters for the LF- and TJ-Monopix prototypes. For Monopix2 also the expected values are given. Entries with a dash (−) indicate that these parameters have not yet been measured for the Monopix2 chips.

	LFoundry			**TowerJazz**		
	Monopix1 measured	Monopix2 expected	Monopix2 measured	Monopix1 measured	Monopix2 expected	Monopix2 measured
Noise	$150 - 200\,e^-$	$100 - 150\,e^-$	$90 - 130\,e^-$	$\sim 20\,e^-$	$< 10\,e^-$	$20\,e^-$
Threshold dispersion	$100\,e^-$	$80\,e^-$	$100\,e^-$	$\sim 30\,e^-$	$< 20\,e^-$	$5\,e^-$
Minimum threshold	$1500\,e^-$	$1000\,e^-$	$\sim 1000\,e^-$	$\sim 300\,e^-$	$< 150\,e^-$	$< 150\,e^-$
In-time threshold	$2000\,e^-$	$1500\,e^-$	–	$\sim 400\,e^-$	$250 - 300\,e^-$	–
Hit efficiency ($10^{15} n_{eq}\mathrm{cm}^{-2}$)	$> 99\%$	$> 99\%$	–	$\sim 70\%$ ($> 98\%^*$)	$> 98\%^*$	–

* for n-gap and 300 μm Czochralski substrate.

pixel tuning works well and reduces the threshold dispersion by more than a factor of 2. The minimum achievable threshold has not yet been determined.

The results obtained for TJ-Monopix2 are preliminary, but indicate that the expected improvements can likely be achieved. The measured ENC is somewhat larger than expected, which is most likely due to cross talk from the digital readout. An overview of TJ-Monopix measurements is given in Tab. 1.

4. Conclusions

The second-generation, full-size DMAPS prototypes Monopix2 arrived in spring 2021 and are currently being tested and characterized. First tests have shown that their synchronous readout architecture in a full-length column is fully functional and that sensors and front-ends show the performance expected from their design improvements. The modifications in pixel layout and front-end design successfully mitigate cross talk. For TJ-Monopix2 it was shown that thanks to process modifications radiation hardness can be achieved with small enough thresholds or the use of a thick Czochralski substrate instead of an epitaxial layer. First results show significant improvements of threshold and noise over the previous version. Further tests and more detailed characterizations of both chips in test beams and after TID and NIEL irradiation are ongoing.

The TJ-Monopix2 prototype has recently been chosen as the baseline for the development of a CMOS sensor for an upgrade of the vertex detector of the Belle II experiment. Its specifications in terms of pixel size, rate capability, timing and radiation tolerance match the requirements for the Belle II upgrade well.

5. Acknowledgments

This project has received funding from the Deutsche Forschungsgemeinschaft DFG (grant WE 976/4-1), the German Federal Ministry of Education and Research BMBF (grant 05H15PDCA9), and the European Union's Horizon 2020 research and innovation programme under grant agreements no. 675587 (Maria Sklodowska-Curie ITN STREAM), 654168 (AIDA-2020), and 101004761 (AIDAinnova). The measurements leading to these results have partially been performed at the Test Beam Facility at DESY Hamburg (Germany), a member of the Helmholtz Association (HGF).

References

[1] R. Turchetta, J. Berst, B. Casadei, G. Claus, C. Colledani, W. Dulinski, Y. Hu, D. Husson, J. Le Normand, J. Riester, G. Deptuch, U. Goerlach, S. Higueret, M. Winter, A monolithic active pixel sensor for charged particle tracking and imaging using standard VLSI CMOS technology, Nuclear Instruments and Methods in Physics Research Section A: Accelerators, Spectrometers, Detectors and Associated Equipment 458 (2001) 677–689.

[2] M. Barbero, et al., Radiation hard DMAPS pixel sensors in 150 nm CMOS technology for operation at LHC, JINST 15 (05) (2020) 05. doi:10.1088/1748-0221/15/05/P05013.

[3] R. Cardella, E. J. Schioppa, K. Moustakas, MALTA: an asynchronous readout CMOS monolithic pixel detector for the ATLAS High-Luminosity

upgrade, Journal of Instrumentation 14 (06 2019). doi:10.1088/1748-0221/14/06/c06019.

[4] M. Kiehn, A. Herkert, A. Weber, A. Schöning, A. Miucci, A. Fehr, C. Blattgerste, C. Grzesik, D. M. S. Sultan, D. Immig, D. Forshaw, D. Ferrere, D. Wiedner, E. Zaffaroni, E. V. Figueras, F. Ehrler, F. Lanni, G. Iacobucci, H. Augustin, H. Liu, H. Chen, I. Peric, J. Anders, J. Hammerich, J. Kröger, J. Vossebeld, K. Chen, L. Xu, L. Noehte, L. Huth, M. Vicente, M. Benoit, M. Weber, M. Prathapan, N. Berger, S. Dittmeier, S. Sevilla, S. Tang, T. Golling, W. Wu, W. Wong, Performance of the ATLASPix1 pixel sensor prototype in ams aH18 CMOS technology for the ATLAS ITk upgrade, JINST 14 (2019) C08013. 7 p. doi:10.1088/1748-0221/14/08/C08013.

[5] The ATLAS Collaboration, Technical Design Report for the ATLAS Inner Tracker Pixel Detector, Tech. rep., CERN-LHCC-2017-021 (2017).

[6] E. Mandelli, L. Blanquart, P. Denes, K. Einsweiler, R. Marchesini, G. Meddeler, M. Ackers, P. Fisher, G. Comes, I. Peric, Digital column readout architecture for the ATLAS pixel 0.25μm front end IC, in: 2001 IEEE Nuclear Science Symposium Conference Record (Cat. No.01CH37310), Vol. 1, 2001, pp. 600–603 vol.1. doi:10.1109/NSSMIC.2001.1008527.

[7] I. Perić, L. Blanquart, G. Comes, P. Denes, K. Einsweiler, P. Fischer, E. Mandelli, G. Meddeler, The FEI3 readout chip for the ATLAS pixel detector, Nuclear Instruments and Methods in Physics Research Section A: Accelerators, Spectrometers, Detectors and Associated Equipment 565 (1) (2006) 178–187, proceedings of the International Workshop on Semiconductor Pixel Detectors for Particles and Imaging. doi:https://doi.org/10.1016/j.nima.2006.05.032.

[8] P. Rymazewski, et al., Development of depleted monolithic pixel sensors in 150 nm CMOS technology for the ATLAS Inner Tracker upgrade, PoS TWEPP-17 (2018) 045. doi:10.22323/1.313.0045.

[9] I. Caicedo, et al., The Monopix chips: Depleted monolithic active pixel sensors with a column-drain read-out architecture for the ATLAS Inner Tracker upgrade, JINST 14 (06) (2019) C06006. doi:10.1088/1748-0221/14/06/C06006.

[10] C. Bespin, et al., DMAPS Monopix developments in large and small electrode designs, Nucl. Instrum. Meth. A 978 (2020) 164460. doi:10.1016/j.nima.2020.164460.

[11] T. Hirono, et al., Depleted fully monolithic active CMOS pixel sensors (DMAPS) in high resistivity 150 nm technology for LHC, Nucl. Instrum. Meth. A 924 (2019) 87–91. doi:10.1016/j.nima.2018.10.059.

[12] K. Moustakas, et al., CMOS Monolithic Pixel Sensors based on the Column-Drain Architecture for the HL-LHC Upgrade, Nucl. Instrum. Meth. A 936 (2019) 604–607. doi:10.1016/j.nima.2018.09.100.

[13] T. Wang, M. Barbero, I. Berdalovic, C. Bespin, S. Bhat, P. Breugnon, I. Caicedo, R. Cardella, Z. Chen, Y. Degerli, N. Egidos, S. Godiot, F. Guilloux, T. Hemperek, T. Hirono, H. Krüger, T. Kugathasan, F. Hügging, C. M. Tobon, K. Moustakas, P. Pangaud, P. Schwemling, H. Pernegger, D.-L. Pohl, A. Rozanov, P. Rymaszewski, W. Snoeys, N. Wermes, Depleted fully monolithic CMOS pixel detectors using a column based readout architecture for the ATLAS Inner Tracker upgrade, Journal of Instrumentation 13 (03) (2018) C03039–C03039. doi:10.1088/1748-0221/13/03/c03039.

[14] K. Moustakas, Design and Development of Depleted Monolithic Active Pixel Sensors with Small Collection Electrode for High-Radiation Applications, Ph.D. thesis, Rheinische Friedrich-Wilhelms-Universität Bonn (Sep. 2021).
URL `https://hdl.handle.net/20.500.11811/9315`

[15] W. Snoeys, G. Aglieri Rinella, H. Hillemanns, T. Kugathasan, M. Mager, L. Musa, P. Riedler, F. Reidt, J. Van Hoorne, A. Fenigstein, T. Leitner,

A process modification for CMOS monolithic active pixel sensors for enhanced depletion, timing performance and radiation tolerance, Nuclear Instruments and Methods in Physics Research Section A: Accelerators, Spectrometers, Detectors and Associated Equipment 871 (2017) 90–96. doi:https://doi.org/10.1016/j.nima.2017.07.046.

[16] H. Pernegger, R. Bates, C. Buttar, M. Dalla, J. van Hoorne, T. Kugathasan, D. Maneuski, L. Musa, P. Riedler, C. Riegel, C. Sbarra, D. Schaefer, E. Schioppa, W. Snoeys, First tests of a novel radiation hard CMOS sensor process for Depleted Monolithic Active Pixel Sensors, Journal of Instrumentation 12 (06) (2017) P06008–P06008. doi:10.1088/1748-0221/12/06/p06008.

[17] M. Dyndal, V. Dao, P. Allport, I. A. Tortajada, M. Barbero, S. Bhat, D. Bortoletto, I. Berdalovic, C. Bespin, C. Buttar, I. Caicedo, R. Cardella, F. Dachs, Y. Degerli, H. Denizli, L. F. S. de Acedo, P. Freeman, L. Gonella, A. Habib, T. Hemperek, T. Hirono, B. Hiti, T. Kugathasan, I. Mandić, D. Maneuski, M. Mikuž, K. Moustakas, M. Munker, K. Oyulmaz, P. Pangaud, H. Pernegger, F. Piro, P. Riedler, H. Sandaker, E. Schioppa, P. Schwemling, A. Sharma, L. S. Argemi, C. S. Sanchez, W. Snoeys, T. Suligoj, T. Wang, N. Wermes, S. Worm, Mini-MALTA: radiation hard pixel designs for small-electrode monolithic CMOS sensors for the High Luminosity LHC, Journal of Instrumentation 15 (02) (2020) P02005–P02005. doi:10.1088/1748-0221/15/02/p02005.

[18] H. Pernegger, P. Allport, I. Asensi Tortajada, M. Barbero, P. Barrillon, I. Berdalovic, C. Bespin, S. Bhat, D. Bortoletto, P. Breugnon, C. Buttar, R. Cardella, F. Dachs, V. Dao, Y. Degerli, H. Denizli, M. Dyndal, L. Flores Sanz de Acedo, P. Freeman, L. Gonella, A. Habib, T. Hemperek, T. Hirono, B. Hiti, T. Kugathasan, I. Mandić, M. Mikuž, K. Moustakas, M. Munker, K. Oyulmaz, P. Pangaud, F. Piro, P. Riedler, H. Sandaker, E. Schioppa, P. Schwemling, A. Sharma, L. Simon Argemi, C. Solans Sanchez, W. Snoeys, T. Suligoj, T. Wang, N. Wermes, Radiation hard

monolithic CMOS sensors with small electrodes for High Luminosity LHC, Nuclear Instruments and Methods in Physics Research Section A: Accelerators, Spectrometers, Detectors and Associated Equipment 986 (2021) 164381. doi:https://doi.org/10.1016/j.nima.2020.164381.

[19] M. Munker, M. Benoit, D. Dannheim, A. Fenigstein, T. Kugathasan, T. Leitner, H. Pernegger, P. Riedler, W. Snoeys, Simulations of CMOS pixel sensors with a small collection electrode, improved for a faster charge collection and increased radiation tolerance, Journal of Instrumentation 14 (05) (2019) C05013–C05013. doi:10.1088/1748-0221/14/05/c05013.